Journal of Photochemistry and Photobiology 6 (2021) 100019

Contents lists available at ScienceDirect

Journal of Photochemistry and Photobiology

journal homepage: www.elsevier.com/locate/jpap

New insights into the Ar-matrix-isolation FTIR spectroscopy and photochemistry of dichloroacetyl chloride, $ClC(O)CHCl_2$: Influence of O_2 and comparison with gas-phase photochemistry

Luciana M. Tamone, A. Lorena Picone, Rosana M. Romano*

CEQUINOR (UNLP, CCT-CONICET La Plata, associated with CIC). Departamento de Química, Facultad de Ciencias Exactas, Universidad Nacional de La Plata. Blvd. 120 N° 1465, La Plata (CP 1900), Argentina.

ARTICLE INFO

Keywords:
Dichloroacetyl chloride
Matrix-isolation
Photochemistry
IR spectroscopy
Dimers

ABSTRACT

Photolysis products of dichloroacetyl chloride (DCAC) isolated in Ar matrix and in gas phase, in the absence and presence of molecular oxygen, were studied by means of FTIR spectroscopy. The samples were exposed to light of different energy ranges (200–800, 280–320, 350–450 and 400–800 nm). DCAC is photostable when irradiated with light of wavelengths above 400 nm, and gives dichloroketene after photolysis with light between 280–320 and 350–450 nm. Exposure of DCAC to broad-band radiation (200–800 nm) produces dichloroketene as an intermediate photoproduct, and different 1:1 $CHCl_3$:CO molecular complexes after further irradiation. HCl, CO and $CHCl_3$ were detected in gas-phase DCAC photolysis. $ClC(O)CCl_2CCl_2H$ molecule was also proposed, in a mechanism that involve the insertion of:CCl_2 biradical into the C−C bond of DCAC. The photochemical reaction of DCAC with O_2 in Ar matrix gives Cl_2CO and CO_2. The same photoproducts, together with HCl, were observed in the gas-phase photochemical reaction. Additionally, the FTIR spectra of DCAC isolated in solid Ar were fully interpreted in terms of an equilibrium between *syn* (the H−C bond *syn* with respect to the C=O bond) and *gauche* conformers. Some absorptions, which grow as the DCAC:Ar ratio increases, were attributed to dimeric forms. The most stable dimer was predicted by DFT calculations as composed by two DCAC molecules with *syn* conformations, interacting through two H-bonds in a structure with C_i symmetry.

1. Introduction

Our research group have been interested in the study of photochemical reactions under matrix conditions and also in gas phase, particularly for small molecular compounds containing either sulphur or/and halogen atoms (see, for example Ref. [1] and 2 and references cited therein). Comparative analysis of the photoproducts formed both in gas phase and in matrix isolation photochemistry may contribute to a better understanding of the photochemical mechanisms.

In the study of the photochemical reaction of trichloroethene (TCE) with molecular oxygen in Ar and N_2 matrices at cryogenic temperatures, we observed an intermediate photoproduct, which can be assigned to dichloroacetyl chloride (DCAC) [3]. It is known that DCAC is a relevant intermediate in reactions of partially chlorinated ethenes, with important environmental implications, mainly due to its high toxicity. It was detected in the photolysis of TCE in air [4], as well as in the photocatalytic degradation of cis- and trans-1,2-dichloroethylene and TCE on UV irradiated TiO_2 catalyst [5]. DCAC, predominantly in its *gauche* form, was also detected after the photochemical reaction of OH radical with TCE in an Ar matrix [6].

Despite the fact that there is a matrix photochemical study of DCAC [7], and it was also detected as an intermediate in the study of the photochemical reaction of TCE with OH radicals in Ar matrix [6], the IR spectrum of the isolated molecule is not fully described in the literature. A more complete study and analysis of the IR spectrum under matrix condition is necessary to correctly interpret the photochemical matrix reactions in which DCAC appears as a possible intermediate product.

Although several studies regarding the conformational properties of DCAC were reported in the literature [7–15], there is still controversy as to which conformer is the most stable. A gas electron diffraction (GED) analysis [13] concluded that the *syn* conformer, with HCCO dihedral angle of *c.a.* 0°, accounts for approximately 72% of the total population. For the *gauche* conformer this angle can be adjusted with values between 100 and 137°. The best fit of the experimental data was achieved for a torsional angle of 138.2 (5.1)°. Finding that the proportion of conformers was invariant with temperature (between 20 and 119°C), the

* Corresponding author.
E-mail address: romano@quimica.unlp.edu.ar (R.M. Romano).

https://doi.org/10.1016/j.jpap.2021.100019
Received 2 September 2020; Received in revised form 31 December 2020; Accepted 22 January 2021
Available online 29 January 2021

authors concluded that the energy of both conformers should be approximately the same. A vibrational (IR and Raman) study of DCAC in different aggregation states proposes a *gauche/syn* equilibrium in the gas and liquid phases, with the *gauche* conformer being the more stable form [11]. Other vibrational analysis, including matrix isolation experiments, arrived to the conclusion that the *syn* form is the most stable one, but based on an opposite assignment to the previous study [14,15]. In a more recent work, the matrix isolation spectra of DCAC in different host species are presented and the most intense IR absorptions of *syn* and *gauche* rotamers were identified, in part due to their behaviour in the presence of UV irradiation [7].

In this work we perform a new investigation of the matrix-isolation spectra of DCAC and present a complete assignment of the spectra in terms of the *syn-gauche* conformational equilibrium. Dimeric DCAC species were also proposed to explain some features of the IR spectra, in accordance with the prediction of theoretical calculations. Photolysis of DCAC isolated in solid Ar and in gas phase with different energy ranges was investigated and the photolysis mechanisms were proposed. The photochemical reactions of DCAC with molecular oxygen under both conditions were also studied.

2. Material and methods

A commercial sample (Aldrich) of dichloroacetyl chloride (DCAC), $ClC(O)CHCl_2$, was purified by several trap-to-trap condensation *in vacuo*. The matrix gas (AGA) was passed through a trap cooled to approximately –90°C to retain possible traces of impurities. Molecular oxygen (AGA) was used without any further purification.

Gas mixtures of DCAC with argon, DCAC, O_2 and Ar, or DCAC and O_2 in different ratios, were prepared by standard manometric methods. Two different instruments were employed for the matrix experiments. One of them reaches a window temperature *c.a.* 10 K by means of a Displex closed-cycle refrigerator (SHI-APD Cryogenics, model DE-202). The second one (Sumitomo Heavy Industries Ltd., model RDK-408D2) achieves temperatures close to 4 K. In both instrument the window material is CsI, and the matrices were formed using the pulse deposition technique [16–18]. FTIR spectra of each matrix sample were recorded at resolutions of 0.5 or 0.125 cm^{-1} using a Nexus Nicolet instrument equipped with either an MCTB or a DTGS detector (for the ranges 4000-400 or 600–180 cm^{-1}, respectively). Following deposition and IR analysis of the resulting matrices, the samples were exposed to broad-band radiation in the 400−800, 350−450, 280−320, and 200−800 nm spectral ranges from a Spectra-Physics Hg-Xe arc lamp operating at 800 W, combined with different dichroic mirrors and filters. The output from this lamp was limited by a water filter to absorb IR radiation and so minimize any heating effects. The FTIR spectra of the matrices were recorded at different irradiation times in order to monitor closely any change in the spectra. The gas-phase photochemical experiments were monitored *in situ*, collecting FTIR spectra before, during and after the irradiation.

The gas-phase UV-Vis spectrum of DCAC was obtained with the UV/Vis Shimadzu 2600, equipped with a Lo-Ray-Ligh grade blazed holographic diffraction grating monochromator and an R-928 photomultiplier detector. A quartz gas cell with 10 cm optical path length was used.

Quantum chemical calculations were performed using the Gaussian 03 program package [19]. Geometry optimizations were performed using standard gradient techniques by simultaneous relaxation of all the geometrical parameters. The calculated vibrational properties correspond in all cases to potential energy minima with no imaginary frequencies. The bonding properties of the molecular complexes have been interpreted by a natural bond orbital (NBO) analysis in terms of "donor-acceptor" interactions [20]. The UV spectra were calculated with the TD-B3LYP/6-311++G(d,p) approximation.

3. Results and discussion

3.1. Ar-matrix FTIR spectra of $ClC(O)CHCl_2$

The FTIR Ar-matrix spectra of DCAC were fully interpreted in terms of an equilibrium between the *syn* and *gauche* conformers. Additional IR absorptions, which grow as the DCAC:Ar ratio increases, were tentatively assigned to dimeric species.

As mention in the introduction, there was a controversy in the literature regarding the relative stabilities of both stable forms of DCAD: the *syn* rotamer, with the H−C bond *syn* with respect to the C=O bond, and the *gauche* form, with the H−C−C=O dihedral angle close to 138° according to Gas Electron Diffraction studies [13].

In this work we have performed theoretical calculations using different methods and basis sets to: i) calculate the relative free energies of the conformers, necessary to determine the expected percentage of each rotamer; ii) simulate the IR spectrum of each form; iii) compare the relative stabilities and calculated spectra of the dimeric forms with respect to the monomers. All the theoretical models used in this work (B3LYP/6-31++G(d,p), B3LYP/6-311++G(d,p), B3LYP/aug-cc-pVTZ, MP2/6-31+G(d)) predicted the *syn* rotamer as the most stable form. The results are presented as Supplementary Information: Potential energy curve (Fig. S1), molecular models of *syn* and *gauche* DCAC and of both transition states *syn−gauche* and *gauche−gauche* (Fig. S2), energy and free energy differences and relative abundances of the conformers (Table S1).

Although the *syn* conformer is predicted as the most stable form, the *gauche* form presents a degeneracy of 2 (see Fig. S1). The existence of two enantiomeric structures of the *gauche* rotamer, in addition to the small energy difference between *syn* and *gauche* conformers, leads to a relative ratio between the two rotamers close to 50:50. The Ar-matrix isolated spectra of DCAC were interpreted in terms of this quasi-equimolar mixture of conformers, taking into account the predicted differences in the wavenumbers and relative IR intensities of the normal modes of each conformer.

The IR spectra of DCAC isolated in Ar matrices present additional signals, which increase their relative intensities as the DCAC:Ar ratio increased, suggesting the possibility of the presence of dimeric species. For this reason, different dimers of DCAC were theoretically investigated, and their IR spectra simulated and compared with that of the monomers.

The most stable form for the dimer, according to the B3LYP/6-311++G(d,p) approximation, is presented in Fig. 1. The structure belongs to the C_i symmetry point group, and consists of two DCAC subunits, each with *syn* conformations, that interact through two H-bonds formed by the hydrogen atoms of each of the subunits with the oxygen atom of the other subunit. This dimer, which we will symbolized as $(DCAC)_{2\text{-}syn}$, is predicted 2.93 Kcal/mol more stable than the monomers. In a second form, $(DCAC)_{2\text{-}gauche}$ which is also shown in Fig. 1, the two subunits possess *gauche* conformation and interact through a single O•••H hydrogen-bond. Table 1 compiles relevant theoretical data of the two most stables structures of $(DCAC)_2$.

To aid in the interpretation of the experimental IR matrix spectra of DCAC, an IR spectrum composed by contributions of the conformational mixture in the predicted ratio (49% *syn* and 51% *gauche*) together with arbitrary quantities (2%) of each dimer, $(DCAC)_{2\text{-}syn}$, and $(DCAC)_{2\text{-}gauche}$, was simulated (Fig. S3−S9). As will be discussed later in this paper, inspection of these Figures was very helpful in assigning the experimental spectra. A complete list of the vibrational calculated wavenumbers for $(DCAC)_2$ species is presented as Supplementary Information (Table S2). The calculated values for *syn*- and *gauche*-DCAC are also included in Table S2.

Table 2 summarizes the wavenumbers and tentative assignment of the FTIR absorptions observed for DCAC isolated in Ar matrices. The gas-phase IR wavenumbers are also included in the Table for comparison purposes. The matrix spectra were interpreted in terms of two con-

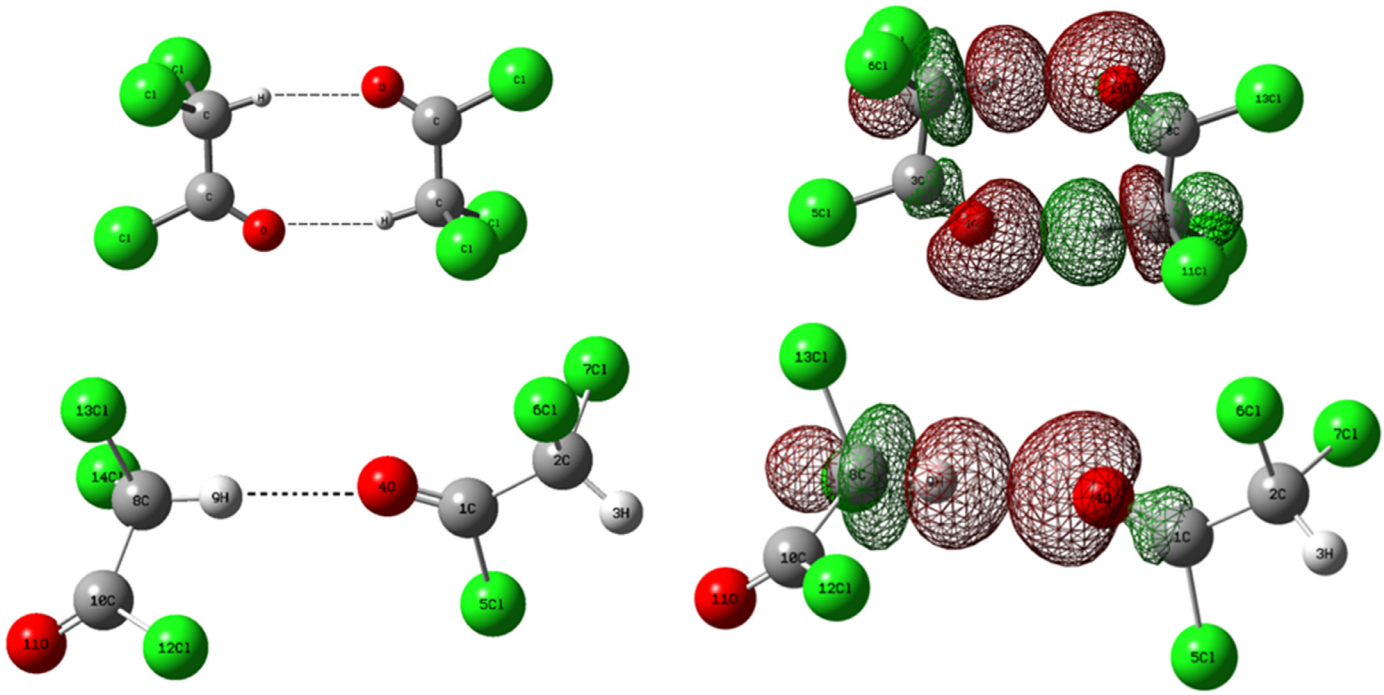

Fig. 1. Top: Molecular models of the optimized dimers of DCAC calculated with the B3LYP/6-311++G(d,p) approximation; left: $(DCAC)_{2\text{-}syn}$; right: $(DCAC)_{2\text{-}gauche}$. Bottom: Schematic representation of the most relevant orbital interactions obtained with the NBO analysis.

Table 1
$\Delta E^{(SCF)}$, ΔE^{CP}, BSSE and GEOM corrections (in kcal.mol^{-1}), transferred charge (q), orbital stabilization energy ($\Delta E^{(2)}$ in kcal.mol^{-1}), H•••O interaction distance (in Å) and penetration distance (in Å) for the dimers of DCAC calculated using the B3LYP/6-311++G(d,p) approximation.

	$(DCAC)_{2\text{-}syn}$	$(DCAC)_{2\text{-}gauche}$
$\Delta E(SCF)$ [a]	−4.00	−2.53
ΔE^{CP} [b]	−2.93	−1.68
BSSE [c]	−1.14	−0.90
GEOM [d]	0.07	0.05
q (e)	0	0.00531
$\Delta E^{(2)}$ [e]	2 x (−1.41) = −2.82 [f]	−1.92
r H•••O	2.3028	2.2942
dp [g]	0.42	0.43

[a] Uncorrected binding energy, $\Delta E^{(SCF)} = E^{AB}_{AB}(AB) - E^{A}_{A}(A) - E^{B}_{B}(B)$, where the subscripts refer to the geometry and the superscript refer to the bases set used to calculate the energy at the geometry defined by the subscript.

[b] Counterpoise corrected binding energy, $\Delta E^{CP} = E^{AB}_{AB}(AB) - E^{AB}_{AB}(A) - E^{AB}_{AB}(B)$

[c] Basis set superposition error correction, $BSSE = E^{AB}_{AB}(A) - E^{A}_{AB}(A) + E^{AB}_{AB}(B) - E^{B}_{AB}(B)$

[d] Geometry correction, $GEOM = E^{A}_{AB}(A) - E^{A}_{A}(A) + E^{B}_{AB}(B) - E^{B}_{B}(B)$

[e] $\Delta E_{n\sigma^*}(DCAC \cdots DCAC) = -2\frac{n_O|\hat{F}|\sigma^*_{C-H}}{(\varepsilon_{\sigma^*_{C-H}} - \varepsilon_{n_O})}$

[f] For $(DCAC)_{2\text{-}syn}$ the orbital stabilization energy is duplicated because each monomer acts simultaneously as electron density donor and acceptor.

[g] Calculated van der Waals penetration distance, $d_p = (\Sigma r_{vdW} - r(H\cdots O))$. $\Sigma r_{vdW} = 2.72$ Å [Ref. 21]

formers described above, *syn* and *gauche*, and by small amounts of at least one dimeric structure.

The carbonylic spectral region is one of the most relevant for the identification of each of the rotamers and the dimeric forms. The band around 1783 cm^{-1} was attributed to the *syn* form, while the signal close to 1816 cm^{-1} was assigned to the *gauche* conformer. The proposed assignment is in agreement with previous reports [7,11], but opposed to others [14,15]. These two bands present distinctive behaviour as a function of irradiation. At the beginning of the irradiation, the intensity of the *gauche* signal increases at the expense of the intensity of the *syn* band, as can be seen in Fig. 2. This light-induced interconversion process between conformers was frequently observed in matrices (see, for example, Ref. [23]). In the present study, this phenomenon was used to correctly identify the bands corresponding to each of the rotamers.

Besides the absorptions of *syn* and *gauche* conformers, the $\nu(C{=}O)_{out\text{-}of\text{-}phase}$ of the $(DCAC)_{2\text{-}syn}$ was associated with a group of bands appearing red-shifted with respect to the monomer, around 1773 cm^{-1}. For this structure, belonging to *Ci* symmetry point group, only one of the two carbonylic vibrational modes is IR active. The second form, $(DCAC)_{2\text{-}gauche}$, presents two vibrational modes in this region; one of them is predicted very close to the monomer, and the second one is red-shifted with respect to the monomer, according with the theoretical calculation. The band at 1814 cm^{-1}, which exhibits characteristic dimer behaviour, was tentatively assigned to $(DCAC)_{2\text{-}gauche}$. In fact, the assignment of this broad-band to a multimer species cannot be completely discarded. Fig. 3 shows the FTIR spectra in the carbonylic stretching region of two different matrices with 1:1000 and 2:1000 DCAC:Ar ratios. The absorptions tentatively assigned to dimeric forms enhance with respect to bands of the monomers as the DCAC proportion in the matrix increases. This relative enhancement was also observed for a matrix hold at ∼ 30 K, corroborating the tentative assignment.

A complete list of the IR absorptions observed in the Ar-matrix spectra, together with their tentative assignment, is compiled in Table 2. Selected regions of the Ar-matrix spectra of DCAC are presented in Fig. S10 and S11.

3.2. Electronic spectra of $ClC(O)CHCl_2$

To the best of our knowledge, there are no reports in the literature on the UV-visible spectrum of DCAC. For this reason, the UV-visible spectrum of the vapour of DCAC, between 190 and 900 nm, was measured using a gas cell with 10 cm optical path. The cell was charged with the vapour pressure of the compound at 22 °C (approximately 30.5 mbar). The spectrum is shown in Fig. S12 of the Supplementary Information. It presents two peaks, one broad absorption at 258.5 nm ($A = 0.12$) and a second one at 195.5 nm ($A = 0.61$). The electronic spectra of both conformers were simulated with the TD-B3LYP/6-311++G(d,p) approxima-

Table 2
Experimental IR wavenumbers (in cm^{-1}) observed in the Ar matrix and gas phase FTIR spectra of dichloroacetyl chloride and calculated (B3LYP/6-311++G(d,p)) wavenumbers and IR intensities (in $Km.mol^{-1}$, between parentheses).

Ar-Matrix	Gas-Phase	Wavenumbers reported previously	B3LYP/6-311++G(d,p) [a]	Tentative Assignment [b]
3035			3074.3 (57)	ν C–H $(DCAC)_2$-*gauche*
			3064.4 (106)	ν C–H $(DCAC)_2$-*syn*
	3014			
3023.6	3010	3010 [c]	3062.8 (3)	ν C–H *gauche*
3010.2	3006		3057.3 (2)	ν C–H *syn*
1818.1	A/C 1826	A/C 1826 [c] / 1816 [d]	1832.1 (272)	ν C=O *gauche*
1815.8	1822	1822		
	1817			
1814.0			1814.9 (378)	ν C=O $(DCAC)_2$-*gauche*
1784.4	A 1795	A/C 1795	1791.1 (314)	ν C=O *syn*
1783.8	1789	1788 [c] / 1784 [d]		
1783.5	1781	1781		
1782.4				
1773.6			1772.8 (871)	ν C=O $(DCAC)_2$-*syn*
1772.0				
1265.6	A 1264	A 1265	1242.4 (7)	$\delta_{in\text{-}plane}$ HCC *gauche*
1259.6	1259	1260 [c]		
	1255	1256		
1229.8	1234	C 1234 [c]	1225.6 (12)	$\delta_{in\text{-}plane}$ HCC *syn*
1226			1245.0 (5)	δ HCC $(DCAC)_2$-*gauche*
1223.8	1228	C 1228 [c]	1216.7 (18)	$\delta_{out\text{-}of\text{-}plane}$ HCC *syn*
		1224		
1220.7	1213	B 1217 [c]	1201.3 (17)	$\delta_{out\text{-}of\text{-}plane}$ HCC *gauche*
1086.2	B 1080	Q,C (?)[e] 1077 [c]	1026.4 (144)	ν C–C *syn*
1082.6	1076			
1071.9				
1078			1028.5 (336)	ν C–C $(DCAC)_2$-*syn*
995			945.1 (110)	ν C–C $(DCAC)_2$-*gauche*
			941.6 (96)	ν C–C $(DCAC)_2$-*gauche*
992.7	996	A 998 [c]	938.2 (106)	ν C–C *gauche*
989.7	992	990		
	987			
797.6	816	802 [c]	756.0 (55)	ν_{as} CCl_2 *gauche*
	808		755.3 (58)	ν_s CCl_2 *syn*
796.5	808		754.9	ν_{as} $CCl^{37}Cl$ *gauche*
			754.6	ν_{as} $C^{37}Cl_2$ *gauche*
795.1			754.4	ν_s $CCl^{37}Cl$ *syn*
			753.0	ν_s $C^{37}Cl_2$ *syn*
786.5		810 [c]	750.2 (105)	ν_{as} CCl_2 *syn*
785.1			749.2	ν_{as} $CCl^{37}Cl$ *syn*
783.8			748.5	ν_{as} $C^{37}Cl_2$ *syn*
741.1	758	759 [c]	728.7 (79)	(ν C–Cl; ν_s CCl_2) *gauche*
739.3				
740.2			727.6	(ν C–Cl; ν_s $C^{37}ClCl$) *gauche*
738.3				
735			703.0 (171)	(ν C–Cl; ν_s CCl_2) $(DCAC)_2$-*gauche*
733.6	743	740 [c]	697.8 (214)	(ν C–Cl; ν_s CCl_2) *gauche*
	740			
732.1			697.0	(ν C–^{37}Cl; ν_s CCl_2) *gauche*
			695.7	(ν C–^{37}Cl; ν_s $C^{37}ClCl$) *gauche*
730.9			695.1	(ν C–^{37}Cl; ν_s $C^{37}Cl_2$) *gauche*
635			605.0 (88)	δ ClCO $_{out\text{-}of\text{-}plane}$ $(DCAC)_2$-*syn*
631.2	640	Q, C 639 [c]	600.0 (49)	δ ClCO $_{out\text{-}of\text{-}plane}$ *syn*
619.0			577.2 (33)	δ ClCO $_{out\text{-}of\text{-}plane}$ *gauche*
585.4			556.1 (250)	ν C–Cl $_{out\text{-}of\text{-}phase}$ $(DCAC)_2$-*syn*
583.5	591	Q, C 587 [c]	553.9 (101)	ν C–Cl *syn*
	587			
580.5			551.4	ν C–^{37}Cl *syn*
500.9	A 508	A 508	482.7 (7)	δ ClCO *syn*
500.2	503	503 [c]		
	497	497		
498.5			479.7	δ ^{37}ClCO *syn*
497.8				

(*continued on next page*)

Table 2 (*continued*)

Ar-Matrix	Gas-Phase	Wavenumbers reported previously	B3LYP/6-311++G(d,p) [a]	Tentative Assignment [b]
461.2	459 455	A 463 460 [c] 454	435.7 (15)	δ ClCO *gauche*
458			430.7	δ ^{37}ClCO *gauche*

[a] scaled by the 0.967 factor [22].
[b] ν stretching, ν_s symmetric stretching, ν_{as} antisymmetric stretching, δ deformation.
[c] gas-phase data from reference [11].
[d] Ar-matrix data from reference [7].
[e] the question mark is transcribed from reference [11].

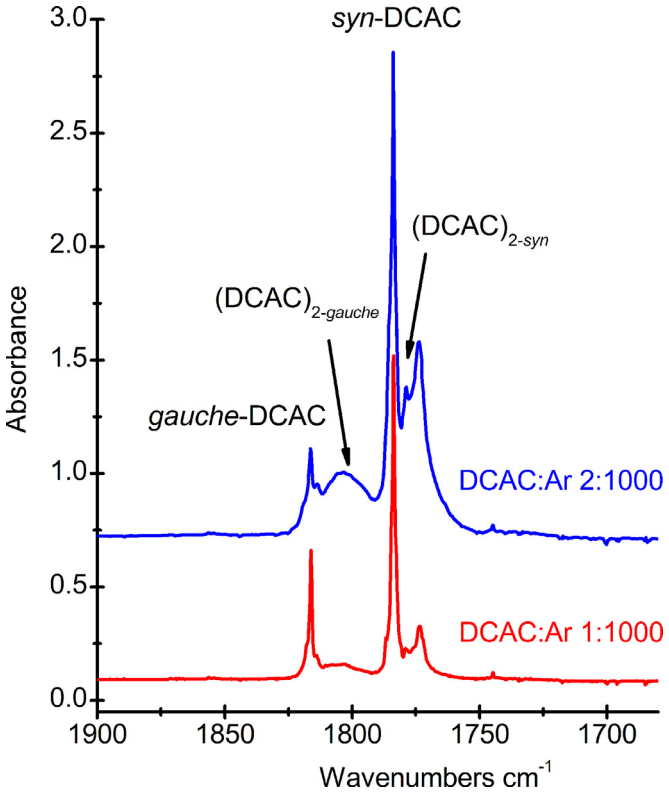

Fig. 3. FTIR spectra of an Ar matrix containing DCAC in 1:1000 (bottom, red-trace) and 2:1000 (top, blue-trace) DCAC:Ar proportions between 1900 and 1680 cm^{-1}. The spectra were taken after 26 and 20 pulse-deposits for the 1:1000 and 2:1000, respectively, with 0.5 cm^{-1} resolution and 64 scans.

tion. The results are in very good agreement with the experimental spectrum. Fig. S13 depicts the calculated UV spectrum of each conformer, as well as the weighted sum of the spectra, taken into account the predicted proportion of the rotamers. The calculated HOMO-LUMO transitions are predicted at 263.9 nm for the *syn* form and at 260.2 nm for the *gauche* conformer. They were assigned to the $\pi_{C=O} \rightarrow \pi^*_{C=O}$ transitions. The second and third peaks are around 220 nm, and arise from $np_{Cl} \rightarrow \pi^*_{C=O}$ transitions. The experimental and calculated data of the UV spectra are collected in Table S3. A schematic representation of the molecular orbital involved in the electronic transitions discussed is placed as Supplementary Information (Fig. S14).

3.3. Photolysis of $ClC(O)CHCl_2$ in Ar matrix and in gas phase

The photolysis of DCAC isolated in Ar with light of different wavelength ranges was studied and the results compared with a previous report [7]. Exposure to visible light ($\lambda \geq 400$ nm) produces no changes in the FTIR matrix spectra. This is consistent with the absence of bands in the UV-visible spectrum of DCAC in this spectral region. Photolysis with radiation in the 350−450 nm wavelength range conducts to the formation of dichloroketene ($Cl_2C=C=O$) as the only photoproduct. Dichloroketene was identified by comparison of the appearing IR absorptions with literature values [24], as presented in Table 3. A selected IR spectrum is presented in Fig. S15. The irradiation of the matrix with light between 280 and 320 nm wavelengths conducts to the same single product. There are no signals in the irradiated matrix spectra attributable to either free or complexed HCl.

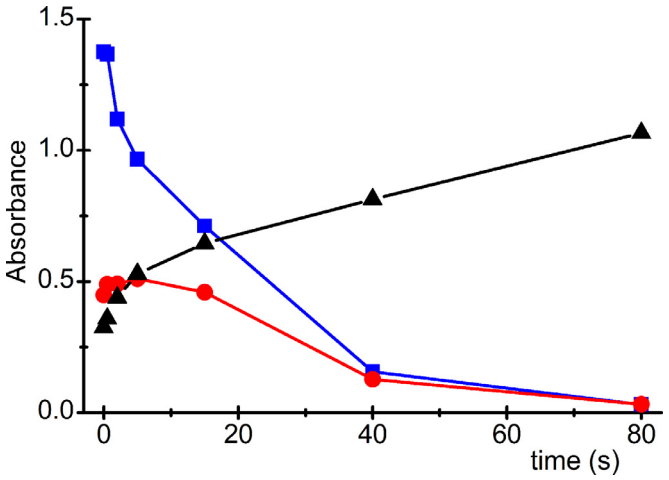

Fig. 2. Plot of the integrated intensities of the IR absorptions centred at 1783 cm^{-1} (*syn* form, squares, blue-trace) and 1816 cm^{-1} (*gauche* form, circles, red-trace) in the Ar-matrix spectra of DCAC (DCAC:Ar 1:1000) as a function of the time of irradiation with broad-band UV-visible light (200 ≤ λ ≤ 800 nm). Relative intensity *gauche/syn* is also plotted (triangles, black-trace).

Table 3
Wavenumbers and assignments of the IR absorptions appearing after photolysis of DCAC isolated in Ar matrix assigned to dichloroketene, $Cl_2C=C=O$

ν (cm^{-1})	Assignment	Wavenumbers reported previously (cm^{-1})
2156.4 2154.9 }	ν (C=O) (ν_1)	2158 [24] 2155/2151 [25]
1292.8	ν (C=C) (ν_2)	1291 [24] 1293/1287 [25]
934.3	ν_{as} (CCl_2) (ν_5)	936 [24] 936/934 [25]
932.6	ν_{as} ($CCl^{37}Cl$)	–
930.9	ν_{as} ($C^{37}Cl_2$)	–
618	δ_{ip} (C=C=O) (ν_6)	605 [24]
526.0	ν_s (CCl_2) (ν_3)	529/520 [24]
418	δ_{oop} (C=C=O) (ν_8)	441 [24]

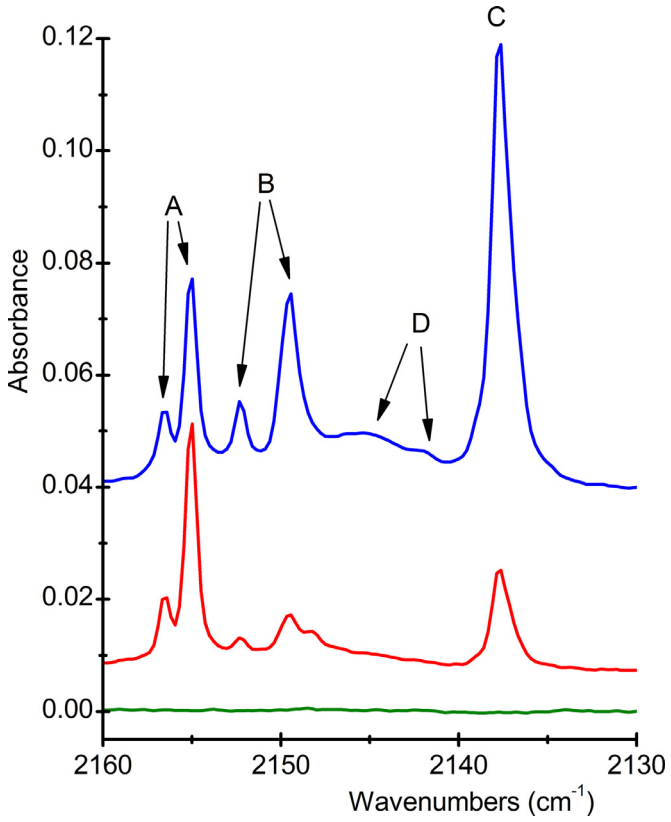

Fig. 4. FTIR spectra of an Ar matrix initially containing DCAC in 1:1000 proportion between 2160 and 2130 cm^{-1} immediately after deposition (bottom, green-trace) and after 2 (middle, red-trace) and 12 min (top, blue-trace) of broad-band UV-visible photolysis. The spectra were taken with 0.5 cm^{-1} resolution and 64 scans. The photoproducts are indicated in the Figure: A) $Cl_2C{=}C{=}O$; B) $Cl_3CH{\bullet\bullet\bullet}CO$; C) $Cl_3CH{\bullet\bullet\bullet}OC$; D) $Cl_2HCCl{\bullet\bullet\bullet}CO$.

Photolysis with UV-visible broad-band radiation gives rise to different photoproducts, with different kinetic behaviours (see Fig. S16–S18 in the Supplementary Material). As presented above in this paper, there is a randomization process between the two conformers, the most stable *syn* form being partially transformed in the *gauche* rotamer (see Fig. 2). Dichloroketene behaves like an intermediate photoproduct that is first formed and then consumed after further photolysis (see Fig. 4). The rest of the IR absorptions that appear as a consequence of UV-visible broad-band irradiation can be attributed to CO and $CHCl_3$, and were tentatively interpreted in terms of different molecular complexes between these two molecules. Ito has studied mixtures of chloroform and carbon monoxide in Ar matrices, and has identified the ν (C–H) and ν (C=O) IR absorptions of the $Cl_3CH{\bullet\bullet\bullet}CO$ stable molecular complex. Moreover, he has assigned another ν (C–H) IR feature to a metastable $Cl_3CH{\bullet\bullet\bullet}OC$ isomer. In this paper, more information about these two forms and also other possible complexes between CO and $CHCl_3$ could be obtained mainly due to: i) DCAC photolysis produces only complexed CO while in the experiment of Ito the ν (C=O) IR absorptions of the complexes (not shown in the paper) are probably obscured by the free CO absorption; ii) photolysis of a matrix-isolated species can give rise to unstable products, whereas in Ito´s experience only thermodynamically stable structures can be formed (see for example Ref [26] in where different complexes were prepared by these two different ways). The assignment of the IR absorptions to the different complexes was performed taking into consideration their distinctive behaviour against irradiation times and also by comparison with theoretical calculations. Not only the two complexes proposed by Ito, but also those formed by the interaction of one of the chloroform chlorine atoms with the carbon or oxygen atom of carbon monoxide, were considered. Table 4 lists the IR wavenumbers tentatively assigned to 1:1 $CHCl_3$/CO molecular complexes, and Fig. 4 depicts selected regions of the IR spectra after different irradiation times.

Table 4
Wavenumbers and tentative assignment of the IR absorptions appearing after photolysis of DCAC isolated in Ar matrix assigned to 1:1 molecular complexes between $CHCl_3$ and CO

ν (cm^{-1})[a]	Assignment Vibrational mode	Complex	Wavenumbers reported previously [27] (cm^{-1})
3059.5	ν (C–H)	$Cl_3CH{\bullet\bullet\bullet}CO$	3059
3053.7	ν (C–H)	$Cl_3CH{\bullet\bullet\bullet}OC$	3063
2152.0, 2149.4	ν (C=O)	$Cl_3CH{\bullet\bullet\bullet}CO$	2149
2145, 2142	ν (C=O)	$Cl_2HCCl{\bullet\bullet\bullet}CO$	-
2137.6	ν (C=O)	$Cl_3CH{\bullet\bullet\bullet}OC$	-
2101.8	ν (^{13}C=O)	$Cl_3CH{\bullet\bullet\bullet}CO$	-
2090.5	ν (^{13}C=O)	$Cl_3CH{\bullet\bullet\bullet}OC$	-
1233.8	δ (C–H)	$Cl_3CH{\bullet\bullet\bullet}CO$	1236
1223.2	δ (C–H)	$Cl_3CH{\bullet\bullet\bullet}OC$	-
769.2, 764.0, 763.0	ν_{as} (CCl_2)	$Cl_3CH{\bullet\bullet\bullet}CO$	-
767.0	ν_{as} (CCl_2)	$Cl_3CH{\bullet\bullet\bullet}OC$	-
673.5, 672.0, 670.7 [b]	ν_s (CCl_3)	$Cl_3CH{\bullet\bullet\bullet}OC$	-
672.3, 670.8, 668.4 [b]	ν_s (CCl_3)	$Cl_3CH{\bullet\bullet\bullet}CO$	-

[a] IR wavenumbers of $CHCl_3$ and CO in Ar matrices measured in the same experimental conditions. $CHCl_3$: 3052.9; 1223.4; 1215.9; 766.1/764.9/763.6; 673.1/671.6/669.9 cm^{-1}. CO: 2138.2 cm^{-1}.
[b] Relative 3:3:1 intensity characteristic of a vibrational mode involving 3 chlorine atoms.

Results of calculated properties of 1:1 $CHCl_3$:CO molecular complexes are placed as Supplementary Information (Table S4 compiles energetic and structural properties, Table S5 lists the calculated vibrational wavenumbers and Fig. S19 presents calculated molecular models of the complexes).

According to the photoproducts detected in the FTIR spectra, the DCAC photolysis mechanisms in Ar matrix can be described by Eq. (1–3). First both, the chlorine atom bonded to the carbonyl group and the hydrogen atom, are released leading to the formation of dichloroketene (Eq. 1). The absence in the FTIR spectra of signal attributed to HCl or complexed HCl is consistent with the idea that H and Cl atoms are probably associated with dichloroketene molecule through weak interactions. This is the only photolysis mechanism in the 350–450 and 280–320 nm spectral range. This process can be associated with $\pi_{C=O} \rightarrow \pi^*_{C=O}$ transitions of both conformers. Although the absorption maximum of the gas-phase UV-visible spectrum of DCAC is above the photolysis energy ranges, the peak is very broad. Also, It is very important to note that the Ar matrix cage effect can slightly shift the UV absorption maxima. This effect is responsible for the wavenumbers shifts of the IR absorptions in the Ar matrix IR spectrum with respect to the gas-phase spectrum (see Table 2).

For UV-visible broad-band photolysis ($200 \leq \lambda \leq 800$ nm), dichloroketene is an intermediate. The experimental finding were interpreted through Eq (2–3). Dichloroketene decomposes into carbon monoxide and the biradical dichlorocarbene (Eq.2). Subsequently, Cl_2C: reacts with the Cl and H atoms previously produced by Eq. 1 to give chloroform, which forms different molecular complexes with CO, also present in the same matrix cage (Eq. 3).

$$HCl_2CC(O)Cl \xrightarrow[matrix]{h\nu} Cl_2C{=}C{=}O + H\cdot + Cl\cdot \quad (1)$$

$$Cl_2C=C=O \xrightarrow[matrix]{h\nu} C\equiv O + Cl_2C: \quad (2)$$

$$C\equiv O + Cl_2C: + H\cdot + Cl\cdot \xrightarrow[matrix]{h\nu} Cl_3CH\cdots C\equiv O \quad (3)$$

The photolysis mechanisms using a broad-band light can be explained by considering the simulated UV spectrum of dichloroketene, calculated also with the TD-B3LYP/6-311++G(d,p) approximation, which predicts a peak around 228 nm. This explains that dichloroketene remains stable for irradiation in the 350–450 and 280–320 nm energy ranges, but photolyzes with light between 200 and 800 nm.

The photolysis of DCAC was also studied in gas phase, with *in-situ* detection of the changes occurred in the FTIR spectra. The first photoproducts clearly observed in the spectra after irradiation with UV-visible Broad-band photolysis were HCl and CO. As the precursor DCAC was consumed, several new IR bands became noticeable. The absorptions at ~772 and 1220 cm^{-1}, with characteristic band-shapes, were associated with the chloroform molecule by comparison with gas-phase FTIR spectra of a $CHCl_3$ taken with the same instrumental conditions. However, the bands at 1805, 1027, 780/777/774 (A-type) and 742/747 (B-type) cm^{-1} could not be assigned to any product with known IR spectrum. Taking into account the Ar-matrix photolysis mechanisms, and also that in the gas phase the mechanisms are not necessarily restricted to unimolecular processes, the insertion of a dichlorocarbene biradical in the C–C single bond of DCAC was tentatively proposed. Although the $ClC(O)CCl_2CCl_2H$ molecule was previously reported [28–30], no IR spectrum could be found in the literature. Eq. 4–6 describe the proposed photolysis mechanisms of DCAC in gas phase. An alternative photochemical channel is presented in Eq. 7, and corresponds to the extrusion of the CO molecule, with the concomitant formation of chloroform, in a unimolecular mechanism. The relative importance of the concerted unimolecular mechanism was increased when selected spectral ranges were used for the photolysis, particularly for the irradiation of the gaseous sample with light in the range of 280 to 320 nm wavelengths.

$$HCl_2CC(O)Cl \xrightarrow[matrix]{h\nu} Cl_2C=C=O + H-Cl \quad (4)$$

$$Cl_2C=C=O \xrightarrow[gas-phase]{h\nu} C\equiv O + Cl_2C: \quad (5)$$

$$HCl_2CC(O)Cl + Cl_2C: \xrightarrow[gas-phase]{h\nu} HCl_2CCl_2CC(O)Cl \quad (6)$$

$$HCl_2CC(O)Cl \xrightarrow[gas-phase]{h\nu} C\equiv O + Cl_3CH \quad (7)$$

Fig. 5 depicts the integrated absorbance of the vibrorotational bands of the HCl and CO molecules as a function of broad-band UV-visible irradiation time in the DCAC gas-phase FTIR spectra. As can be observed in the Figure, small amounts of HCl are present in the sample as impurity from before irradiation. After 68 min. of photolysis approximately 75 % of DCAC was consumed.

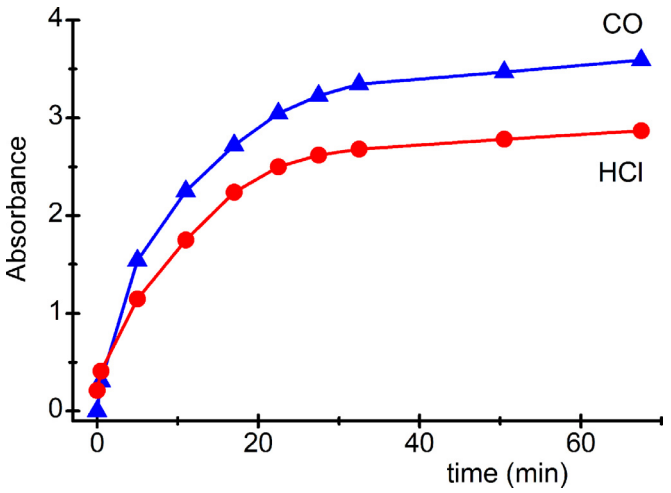

Fig. 5. Plot of the integrated intensities of the IR absorptions of HCl (circles, red-trace) and CO (triangles, blue-trace) as a function of the photolysis time of a gaseous DCAC sample with broad-band UV-visible light ($200 \leq \lambda \leq 800$ nm).

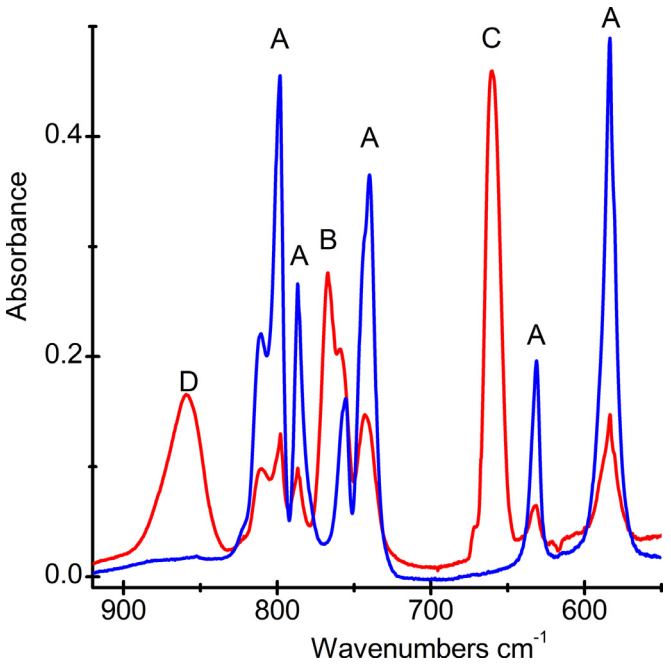

Fig. 6. FTIR spectra of an Ar matrix initially containing DCAC an O_2 in a DCAC:O_2:Ar 1:20:1000 proportion immediately after deposition (blue-trace) and after 50 min (red-trace) of broad-band UV-visible photolysis. The spectra were taken with 0.5 cm^{-1} resolution and 64 scans. The species are indicated in the Figure: A) DCAC; B) $CHCl_3$:CO; C) CO_2 D) Cl_2CO.

3.4. Photochemical reaction of $ClC(O)CHCl_2$ with molecular oxygen in Ar matrix and in gas phase

The main products of the photochemical reaction of DCAC and O_2 in Ar matrix are phosgene, Cl_2CO, and carbon dioxide, as can be observed in Fig. 6. No IR features assignable to HCl or complexed HCl were observed in the IR spectra after photolysis. The main mechanism can be schematized by Eq. 8.

$$HCl_2CC(O)Cl + O_2 \xrightarrow[matrix]{h\nu} Cl_2C=O + CO_2 + H\cdot + Cl\cdot \quad (8)$$

The IR spectra of isolated two-component mixtures in a rigid matrix should be interpreted as consisting of signals arising from different matrix cages, some of which house each of the components individually and others containing two molecules (either the two components or dimers) in the same cage. On irradiation, the content of each type of cage will evolve independently. For this reason, some of the products, formed in cages housing only DCAC, are expected to match those already described for Ar-matrix isolated DCAC. Consistent with this assumption, dichloroketene was detected as intermediate and 1:1 complexes between CO and $CHCl_3$ were also formed (see Fig. 6). As the O_2:DCAC ratio in the matrix increases, the relative intensity of the CO_2 and Cl_2CO absorptions with respect to the Cl_2CCO and $CHCl_3$:CO bands also increases. This fact confirms the mechanism described by Eq. 8 for the DCAC/O_2 photochemical reaction, and that the rest of the photoproducts correspond to the photolysis of isolated DCAC.

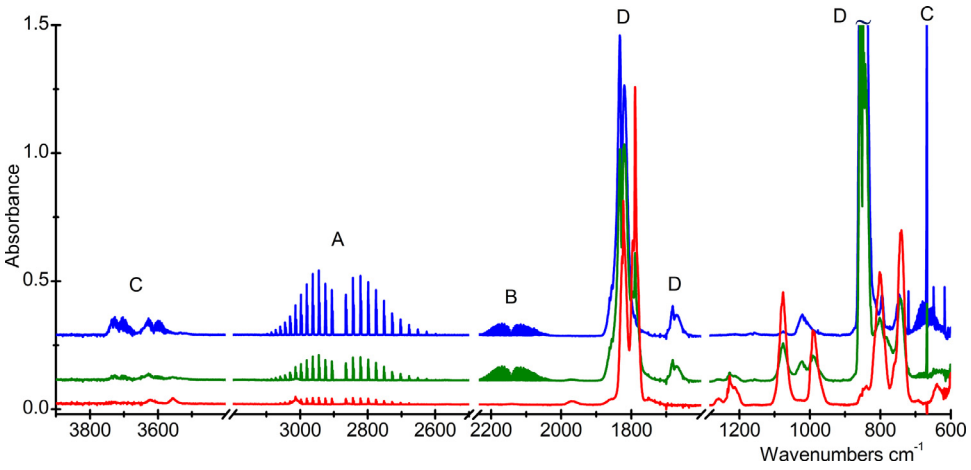

Fig. 7. FTIR spectra of 1:1 DCAC:O_2 gaseous mixture (1 mbar each) before (bottom, green-trace), and after 3 (middle, green-trace) and 14 min (top, blue-trace) of broad-band UV-visible photolysis. The spectra were taken with 1 cm^{-1} resolution and 4 scans. The photoproducts are indicated in the Figure: A) HCl; B) CO; C) CO_2 D) Cl_2CO.

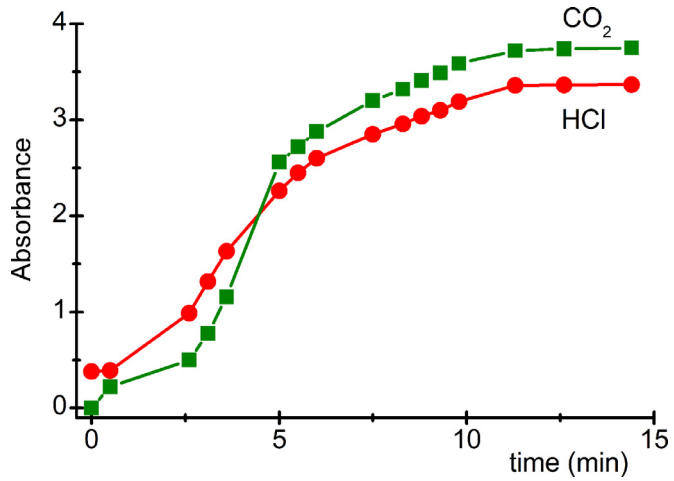

Fig. 8. Plot of the integrated intensities of the IR absorptions of ($\nu_1+\nu_3$) and ($2\nu_2+\nu_3$) combination modes of CO_2 (squares, green-trace) and of HCl fundamental (circles, red-trace) in a 1:1 DCAC:O_2 gaseous mixture (1 mbar each) as a function of the time of irradiation with broad-band UV-visible light ($200 \leq \lambda \leq 800$ nm).

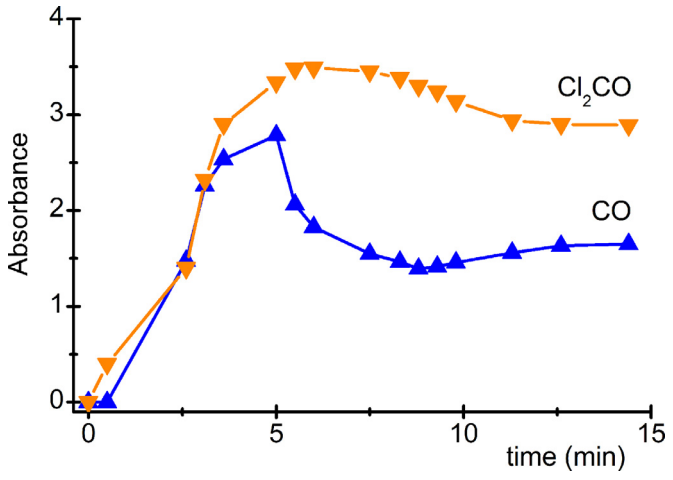

Fig. 9. Plot of the integrated intensities of the IR absorptions of $2\nu_5$ overtone of phosgene (triangles-down, orange-trace) and of CO fundamental (triangles-up, blue-trace) in a 1:1 DCAC:O_2 gaseous mixture (1 mbar each) as a function of the time of irradiation with broad-band UV-visible light ($200 \leq \lambda \leq 800$ nm).

In the photochemical gas-phase reaction between DCAC and O_2 in an equimolar proportion (1 mbar of each of the reactants) using broad-band UV-visible radiation, DCAC is completely consumed after ~10 min. of irradiation. The strongest absorptions appearing in the FTIR spectra after the mixture was exposed to the radiation were attributed to phosgene, carbon dioxide, hydrogen chloride and carbon monoxide (see Fig. 7). The features tentatively assigned to $ClC(O)CCl_2CCl_2H$ molecule in the gas-phase photolysis of DCAC were also observed, and even became clearer after total DCAC consumption due to the partial overlap of the absorptions of both compounds. To help in the interpretation of the photochemical mechanisms, the integrated intensities of the vibro-rotational bands of HCl and CO molecule and selected bands of CO_2 and Cl_2CO were plotted against irradiation time (Fig. 8 and 9). It was not possible to measure the intensity of any $ClC(O)CCl_2CCl_2H$ band due to the partial overlap with absorptions of DCAC and phosgene.

Fig. 8. Plot of the integrated intensities of the IR absorptions of ($\nu_1 + \nu_3$) and ($2\nu_2 + \nu_3$) combination modes of CO_2 (squares, green-trace) and of HCl fundamental (circles, red-trace) in a 1:1 DCAC:O_2 gaseous mixture (1 mbar each) as a function of the time of irradiation with broad-band UV-visible light ($200 \leq \lambda \leq 800$ nm).

The behaviour against irradiation time of CO_2 and HCl suggests that both photoproducts can be form simultaneously (Fig. 8). On the other hand, phosgene photolysis is known to give CO and chlorine atoms [31], which may explain the intermediate behaviour of this photoproduct (Fig. 9). Based on these findings, Eq. 9 can describe the main photochemical reaction mechanism for the reaction between DCAC and molecular oxygen, followed by the photolysis of phosgene (Eq. 10) [31].

$$HCl_2CC(O)Cl + O_2 \xrightarrow[gas-phase]{h\nu} Cl_2C=O + CO_2 + H - Cl \quad (9)$$

$$Cl_2C=O \xrightarrow{h\nu} C \equiv O + 2Cl\cdot \quad (10)$$

The particular behaviour of CO absorption with irradiation time is consistent with more than one mechanism for its production and consumption. Considering that the absorptions tentatively assigned to $ClC(O)CCl_2CCl_2H$ were also observed in the IR spectra, we proposed that the photochannels described by Eq. 4–6, which correspond to DCAC photolysis, also contribute to complete the mechanism scheme. Increasing the proportion of molecular oxygen in the mixtures favours the channel described by Eq. 9 over the DCAC photolysis products and results in an increased reaction rate.

4. Conclusions

The FTIR spectra of dichloroacetyl chloride (DCAC) were fully interpreted in terms of two conformers, *syn* (with the H–C bond *syn* with

respect to the C=O bond) and *gauche* form, and at least one, or probably two, dimeric forms. The complete assignment of the IR absorptions of each of the rotamers was performed based on their behaviour against the UV-visible broad-band irradiation, since the relative intensities of the bands of the *gauche* form increase at the expense of the absorptions of the *syn* form, and the comparison with the simulated IR spectra. The IR bands of the dimeric forms were recognized by their enhancement as the DCAC:Ar proportion increases. The most stable dimeric form, $(DCAC)_{2\text{-}syn}$, is composed by two DCAC molecules with *syn* conformations, which interact through two H-bonds formed by the hydrogen atoms of each of the subunit with the oxygen atom of the other subunit, forming a structure with C_i symmetry.

Photolysis of DCAC isolated in Ar matrix leads to dichloroketene, probably coordinated to H and Cl atoms, as an intermediate photoproduct, which subsequently evolves into the formation of different 1:1 $CHCl_3$:CO molecular complexes with further photolysis. The absence of HCl in the irradiated matrix constitutes a difference with the study previously reported, as well as the lack of ClCO radical in the spectra [7]. $Cl_3CH\cdots CO$ and $Cl_3CH\cdots OC$ molecular complexes were previously described, isolated from a chloroform and carbon monoxide mixture in Ar. In this work, we also proposed the formation of a third less stable structure, $Cl_2HCCl\cdots CO$, which was not previously reported. This is in accordance with the theoretical relative stability of this form that prevents its formation in a mixture of the two components. If the wavelength radiation range is limited either to 350−450 or 280−320 nm, dichloroketene is the only photoproduct. On the other hand, DCAC isolated in solid Ar is stable to visible light.

To the best of our knowledge, the products of the photolysis of DCAC in gas phase were not previously described. In this work, HCl, CO and $CHCl_3$ were detected. Additionally, an unknown compound were tentatively assigned to $ClC(O)CCl_2CCl_2H$ molecule based on the IR signals appearing in the IR spectra during photolysis. The proposed mechanism begins with the formation of hydrogen chloride and dichloroketene. $Cl_2C{=}C{=}O$ immediately decomposes into CO and dichlorocarben biradical. A subsequent insertion of this biradical into the C−C bond of DCAC gives $ClC(O)CCl_2CCl_2H$. A second and less important concerted mechanism forms chloroform and carbon monoxide.

The differences in the photolysis mechanisms of DCAC in Ar matrix and in gas phase can be easily explained. On one hand, the matrix photolysis experiments on highly diluted samples are mainly restricted to unimolecular mechanisms; additionally, it is possible to isolate unstable molecules or high-energy forms. On the other hand, gas-phase photolysis experiments allow mechanisms with higher molecularity, such as in the case of the formation of $ClC(O)CCl_2CCl_2H$.

The photochemical reaction of DCAC with molecular oxygen gives phosgene and carbon dioxide, either in Ar matrix or in gas phase. The main difference is the formation of HCl in gas phase, and the lack of this photoproduct in matrix. The formation of CO in gas phase was mainly attributed to the known photochemical decomposition of phosgene.

Declaration of Competing Interest

The authors declare that they have no known competing financial interests or personal relationships that could have appeared to influence the work reported in this paper.

Acknowledgments

The authors thank Consejo Nacional de Investigaciones Científicas y Técnicas (CONICET), Agencia Nacional de Promoción de la Investigación, el Desarrollo Tecnológico y la Innovación (ANPCyT) (PICT 2014-3266), and Universidad Nacional de La Plata (UNLP X/822) for financial support.

Supplementary materials

Supplementary material associated with this article can be found, in the online version, at doi:10.1016/j.jpap.2021.100019.

References

[1] Y.B. Bava, L.M. Tamone, L.C. Juncal, S. Seng, Y.A. Tobón, S. Sobanska, A.L. Picone, R.M. Romano, Gas-phase and matrix-isolation photochemistry of methyl thioglycolate, $CH_3OC(O)CH_2SH$: influence of the presence of molecular oxygen un the photochemical mechanism, J. Photochem. Photobiol. A. 344 (2017) 101–107, doi:10.1016/j.jphotochem.2017.05.003.
[2] M.V. Cozzarín, R.M. Romano, H. Willner, C.O. Della Védova, Matrix isolation of the elusive fluorocarbonylsulfenyl fluoride molecule FC(O)SF, J. Phys. Chem. A. 117 (2013) 855–862, doi:10.1021/jp309310n.
[3] L.M. Tamone, A.L. Picone, R.M. Romano, unpublished results.
[4] W.R. Haag, M.D. Jhonson, Direct photolysis of trichloroethene in air: efect of cocontaminants toxicity of products and hydrothermal treatment of products, Environ. Sci. Technol. 30 (1996) 414–421, doi:10.1021/es950047y.
[5] K. Oki, S. Tsuchida, H. Nishikiori, N. Tanaka, T. Fujii, Photocatalytic degradation of chlorinated ethenes, Int. J. Photoenergy 5 (2003) 11–15, doi:10.1155/S1110662X03000059.
[6] K.S. Wiltshare, M.J. Almond, P.C.H. Mitchell, Reactions of hydroxyl radicals with trichloroethene and tetrachloroethene in argon matrices al 12 K, Phys. Chem. Chem. Phys. 6 (2004) 58–63, doi:10.1039/B310495H.
[7] N. Tanaka, Matrix isolation and computational study on the photolysis of $CHCl_2COCl$, Open. J. Phys. Chem. 4 (2014) 117–125, doi:10.4236/ojpc.2014.43014.
[8] A. Miyake, I. Nakagawa, T. Miyazawa, I. Ichishima, T. Shimanouchi, S. Mizushima, Infrared and Raman spectra of dichloroacetyl chloride in relation to rotational isomerism, Spectrochim. Acta. 13 (1958) 161–167, doi:10.1016/0371-1951(58)80073-9.
[9] A.J. Woodward, N. Jonathan, Rotational isomerism in dichloroacetyl halides, J. Phys. Chem 74 (1970) 798–805, doi:10.1021/j100699a022.
[10] R. Fausto, J.J.C. Teixeira-Dias, Conformational and vibrational spectroscopic analysis of $CHCl_2COX$ and CCl_3COX (X= Cl, OH, OCH_3), J. Mol. Struct. 144 (1986) 241–263, doi:10.1016/0022-2860(86)85004-9.
[11] J.R. Durig, M. Mamula Bergana, H.V. Phan, Conformational stability, barriers to internal rotation, ab initio calculations and vibrational assignment of dichloroacetyl chloride, J. Mol. Struct. 242 (1991) 179–205, doi:10.1016/0022-2860(91)87135-5.
[12] G.B. Soifer, V.P. Feshin, Molecular structure and conformational transitions of dichloroacetyl chloride, J. Struct. Chem. 47 (2006) 371–374, doi:10.1007/s10947-006-0309-5.
[13] R.L. Quan Shen, K.H. Hilderbrandt, K. Hagen, The structure and conformation of dichloroacetyl chloride as determined by gas-phase electron diffraction, J. Mol. Struct. 71 (1981) 161–169, doi:10.1016/0022-2860(81)85113-7.
[14] A.A. El-Bindary, P. Klaeboe, C.J. Nielsen, The conformational equilibria and vibrational spectra, including infrared matrix isolation spectra, of chloroacetyl bromide, Acta Chem. Scand. 45 (1991) 877–886.
[15] G. Davidovics, A. Allouche, M. Monnier, Ab initio calculations and vibrational assignment of chloroacetyl chloride trapped in a low temperature xenon matrix, J. Mol. Struct. 243 (1991) 1–12.
[16] I.R. Dunkin, Matrix-Isolation Techniques: A Practical Approach, Oxford University Press, New York, 1998.
[17] M.J. Almond, A.J. Downs, Spectroscopy of Matrix Isolated Specie Adv. in Spectroscopy, Chichester, 1989 Volume 17.
[18] R.N. Perutz, J.J. Turner, Pulsed matrix isolation. A comparative study, J. Chem. Soc., Faraday Trans. 2. 69 (1973) 452–461, doi:10.1039/F29736900452.
[19] M.J. Frisch, G.W. Trucks, H.B. Schlegel, et al., Gaussian 03, Revision C.02, Gaussian Inc., Wallingford CT, 2004.
[20] A.E. Reed, L.A. Curtiss, F. Weinhold, Intermolecular interactions from a natural bond orbital, donor-acceptor viewpoint, Chem. Rev. 88 (1988) 899–926, doi:10.1021/cr00088a005.
[21] A. Bondi, Van der Waals Volumes and Radii, J. Phys. Chem. 68 (1964) 441–451.
[22] Computational Chemistry Comparison and Benchmanrk DataBase, National Institute of standards and technology, http://cccbdb.nist.gov/vibscalejust.asp.
[23] R.M. Romano, C.O. Della Védova, A.J. Downs, T.M. Greene, Matrix photochemistry of *syn*-(chlorocarbonyl) sulfenyl bromide, *syn*-ClC(O)SBr; precursor to the novel species *anti*-ClC(O)SBr, *syn*-BrC(O)SCl, and BrSCl, J. Am. Chem. Soc. 123 (2001) 5794–5801, doi:10.1021/ja010252f.
[24] G. Davidovics, M. Monnier, A. Allouche, FT-IR spectral data and ab initio calculations for haloketenes, Chem. Phys. 150 (1991) 395–403, doi:10.1016/0301-0104(91)87112-9.
[25] T. Tamezane, N. Tanaka, H. Nishikiori, T. Fujii, Matrix isolation and theoretical study on the photolysis of trichloroacetyl chloride, Chem. Phys. Lett. 423 (2006) 434–438, doi:10.1016/j.cplett.2006.04.031.
[26] A.L. Picone, C.O. Della Védova, H. Willner, A.J. Downs, R.M. Romano, Experimental and theoretical characterization of molecular complexes formed between OCS and XY molecules (X, Y= F, Cl and Br) and their role in photochemical matrix reactions, Phys. Chem. Chem. Phys. 12 (2010) 563–571, doi:10.1039/b914862k.
[27] F. Ito, Matrix-isolation infrared studies of 1:1 molecular complexes containing chloroform ($CHCl_3$) and Lewis bases: seamless transition from blue-shifted to red-shifted hydrogen bonds, J. Chem. Phys. 137 (2012) 014505, doi:10.1063/1.4730909.

[28] C.W. Theobald, C. Hundred, Process for making polyhalogenated straight-chain aliphatic carboxylic acid halides, United States Patent office (1946) 2411982.
[29] H. Laato, L. Hautoniemi, Preparation of esters of chlorinated propionic acids, Suomen Kem 41 (1968) 266–268.
[30] I.O.O. Korhonen, Gas-liquid chromatographic analyses of chlorination products of propionyl chloride, J. Chromatogr. 213 (1981) 63–71, doi:10.1016/S0021-9673(00)80633-0.
[31] H. Babad, A.G. Zeiler, The Chemistry of phosgene, Chem. Rev. 73 (1973) 75–91, doi:10.1021/cr60281a005.